

Muon-Spin Rotation and Magnetization Studies of Chemical and Hydrostatic Pressure Effects in $\text{EuFe}_2(\text{As}_{1-x}\text{P}_x)_2$

Z. Guguchia · A. Shengelaya · A. Maisuradze ·
L. Howald · Z. Bukowski · M. Chikovani · H. Luetkens ·
S. Katrych · J. Karpinski · H. Keller

Received: 24 July 2012 / Accepted: 30 July 2012 / Published online: 25 August 2012
© Springer Science+Business Media, LLC 2012

Abstract The magnetic phase diagram of $\text{EuFe}_2(\text{As}_{1-x}\text{P}_x)_2$ was investigated by means of magnetization and muon-spin rotation (μSR) studies as a function of chemical (isovalent substitution of As by P) and hydrostatic pressure. The magnetic phase diagrams of the magnetic ordering of the Eu and Fe spins with respect to P content and hydrostatic pressure are determined and discussed. The present investigations reveal that the magnetic coupling between the Eu and the Fe sublattices strongly depends on chemical and hydrostatic

pressure. It is found that chemical and hydrostatic pressures have a similar effect on the Eu and Fe magnetic order.

Keywords High temperature Fe-based superconductor · Localized and band magnetism · Hydrostatic pressure · Chemical pressure

1 Introduction

The discovery of superconductivity in the iron-based pnictides [1] provided a new class of compounds to the high temperature superconductor (HTS) family. Ternary iron arsenide AFe_2As_2 ($A = \text{Sr}, \text{Ca}, \text{Ba}, \text{Eu}$) [2] is one of the parent compounds with ThCr_2Si_2 -type structure. Similarly as LnFeAsO ($\text{Ln} = \text{La}–\text{Gd}$) [3], AFe_2As_2 undergoes a structural phase transition from a tetragonal to an orthorhombic phase, accompanied or followed by a spin-density-wave (SDW) transition of the itinerant Fe moments. The superconducting (SC) state can be achieved either under pressure (chemical and hydrostatic) [4–6] or by appropriate charge carrier doping of the parent compounds [7–9], both accompanied by a suppression of the SDW state.

Here, we focus on EuFe_2As_2 which is a particularly interesting member of the ternary system AFe_2As_2 , since the A site is occupied by a rare earth Eu^{2+} S -state (orbital moment $L = 0$) ion with a $4f^7$ electronic configuration. Eu^{2+} has a total electron spin $S = 7/2$, corresponding to a theoretical effective magnetic moment of $\mu_{\text{eff}} = 7.94 \mu_B$. In addition to the SDW ordering of the Fe moments at $T_{\text{SDW}} \simeq 190 \text{ K}$, an antiferromagnetic (AFM) order of the Eu^{2+} spins at $T_{\text{AFM}} \simeq 19 \text{ K}$ was reported by Mössbauer spectroscopy [10] and later confirmed by neutron diffraction [11]. Various reports on $\text{EuFe}_{2-x}\text{Co}_x\text{As}_2$ ($x = 0$ and 0.1) suggest a strong coupling between the magnetism of the Eu^{2+} ions and the conduction electrons, which may affect or even destroy superconductiv-

Z. Guguchia (✉) · A. Maisuradze · L. Howald · H. Keller
Physik-Institut der Universität Zürich, Winterthurerstrasse 190,
8057 Zürich, Switzerland
e-mail: zurabgug@physik.uzh.ch

A. Shengelaya · M. Chikovani
Department of Physics, Tbilisi State University, Chavchavadze 3,
0128 Tbilisi, Georgia

Present address:

M. Chikovani
Laboratory for Developments and Methods, Paul Scherrer
Institute, 5232 Villigen PSI, Switzerland

A. Maisuradze · H. Luetkens
Laboratory for Muon Spin Spectroscopy, Paul Scherrer Institute,
5232 Villigen PSI, Switzerland

Present address:

Z. Bukowski
Institute of Low Temperature and Structure Research, Polish
Academy of Sciences, 50-422 Wrocław, Poland

Z. Bukowski · S. Katrych · J. Karpinski
Laboratory for Solid State Physics, ETH Zürich, 8093 Zürich,
Switzerland

Present address:

S. Katrych · J. Karpinski
Institut de Physique de la Matière Condensée (ICMP), Ecole
Polytechnique Fédérale de Lausanne (EPFL), 1015 Lausanne,
Switzerland

ity [12, 13]. For example, in contrast to the other ‘122’ systems, where the substitution of Fe by Co leads to superconductivity [14, 15], the compounds containing Eu^{2+} exhibit the onset of a superconducting transition, but seem to be hindered to reach zero resistivity at ambient pressure [16]. Although Ni doping in BaFe_2As_2 leads to superconductivity up to 21 K [17], ferromagnetism rather than superconductivity was found in EuFe_2As_2 by Ni doping [18]. On the other hand, in single crystals of P substituted $\text{EuFe}_2(\text{As}_{1-x}\text{P}_x)_2$ bulk superconductivity with superconducting transition temperature $T_c \simeq 28$ K was observed by resistivity, magnetization, and specific heat measurements [19]. Isovalent P substitution on the As site in EuFe_2As_2 without introducing holes or electrons simulates a condition generally referred to as “chemical pressure”. Superconductivity coexisting with AFM Eu^{2+} order was only found in a very narrow range of P content x ($0.16 \leq x \leq 0.22$), where the SDW transition is suppressed. Superconductivity with a zero resistivity state was also observed for EuFe_2As_2 under applied pressure [6, 20]. Similar to the case of P substitution, superconductivity covers only a narrow pressure range of 2.5–3.0 GPa.

In this paper, we report detailed magnetization and muon spin rotation (μSR) measurements in $\text{EuFe}_2\text{As}_{2-x}\text{P}_x$ as a function of the P content x . One P substituted sample $\text{EuFe}_2(\text{As}_{0.88}\text{P}_{0.12})_2$ was also studied under applied pressure p . The μSR technique is a powerful tool to study the magnetic and superconducting properties of materials microscopically. It provides reliable measurements of T_c , T_{SDW} , the magnetic ordering temperature of Eu^{2+} spins T_{Eu} and the ordered moment size as a function of both x and p . Consequently, the phase diagrams with respect x and p are determined from these measurements. We compare the present results with previous high pressure studies on the parent compound EuFe_2As_2 and discuss the combined results in terms of the relation of x and p . The paper is organized as follows: Experimental details are described in Sect. 2. The results of the magnetic susceptibility and the μSR experiments at ambient and applied pressure are presented and discussed in Sects. 3.1 and 3.2, respectively. In Sect. 4, the phase diagrams are presented. The conclusions follow in Sect. 5.

2 Experimental Details

In the present work, the system $\text{EuFe}_2(\text{As}_{1-x}\text{P}_x)_2$ with $x = 0, 0.12, 0.2$, and 1 is investigated. Note that the sample with $x = 0$ is single crystalline, and all the P substituted compounds are polycrystalline. The concentrations $x = 0.12$ and 0.2 were studied due to their proximity to the SC phase reported in [19]. A single crystal of EuFe_2As_2 was grown out of Sn flux [21]. Polycrystalline samples were synthesized by solid-state reaction between EuAs, Fe_2As , and Fe_2P . EuAs was presynthesized by heating europium grains and phosphorus powders very slowly to 1173 K followed

by a tempering at this temperature for 36 h. Fe_2As was prepared by heating Fe and As powders at 973 K for 10 h and at 1173 K for 15 h. Fe_2P was presynthesized by reacting iron and phosphorus powders at 973 K for 24 h from stoichiometric amounts of the elements. All the starting materials had a purity better than 99.9 %. Powders of EuAs, Fe_2As , and Fe_2P were weighted according to the stoichiometric ratio, thoroughly ground and pressed into pellets in an argon-filled glove box. The pellets were then sealed in an evacuated quartz tube, sintered at 1273 K for 36 h, and then cooled slowly to room temperature.

Powder X-ray diffraction (XRD) studies of the $\text{EuFe}_2(\text{As}_{1-x}\text{P}_x)_2$ samples were carried out at room temperature with a STOE diffractometer ($\text{CuK}\alpha_1$ radiation, $\lambda = 1.5406$ Å) equipped with a mini-phase-sensitive detector and a Ge monochromator. The structural refinements were done using the program FULLPROF [22]. The zero-field-cooled and field-cooled (ZFC and FC) magnetization measurements of the $\text{EuFe}_2(\text{As}_{1-x}\text{P}_x)_2$ samples were performed with a commercial SQUID magnetometer (*Quantum Design* MPMS-XL). The samples with $x = 0.2$ and 1 were studied only at ambient pressure. For $x = 0.12$, the investigations were also carried out under applied pressures up to $p = 5.9$ GPa by using a diamond anvil cell (DAC) filled with Daphne oil which served as a pressure-transmitting medium. The pressure at low temperatures was determined by the pressure dependence of the SC transition temperature of Pb.

Zero-field (ZF) μSR experiments were performed at the μE1 and πM3 beamlines of the Paul Scherrer Institute (Villigen, Switzerland). The general purpose instrument (GPS) was used to study the system $\text{EuFe}_2(\text{As}_{1-x}\text{P}_x)_2$ ($x = 0, 0.12, 0.2$, and 1) at ambient pressure. The samples were mounted inside of a gas-flow ^4He cryostat on a sample holder with a standard veto setup providing a low-background μSR signal. In addition, the sample with $x = 0.12$ was studied under pressure using the GPD instrument. Pressures up to 2.0 GPa were generated in a double wall piston-cylinder type of cell made of MP35N [23] material especially designed to perform μSR experiments under pressure. As a pressure transmitting medium Daphne oil was used. The pressure was measured by tracking the SC transition of a very small indium plate by AC susceptibility. The μSR time spectra were analyzed using the free software package MUSRFIT [24].

3 Results and Discussion

3.1 Crystal Structure and Magnetic Properties of $\text{EuFe}_2(\text{As}_{1-x}\text{P}_x)_2$

3.1.1 X-Ray Powder Diffraction

The crystal structure for all $\text{EuFe}_2(\text{As}_{1-x}\text{P}_x)_2$ samples at room temperature was refined with the tetragonal ThCr_2Si_2

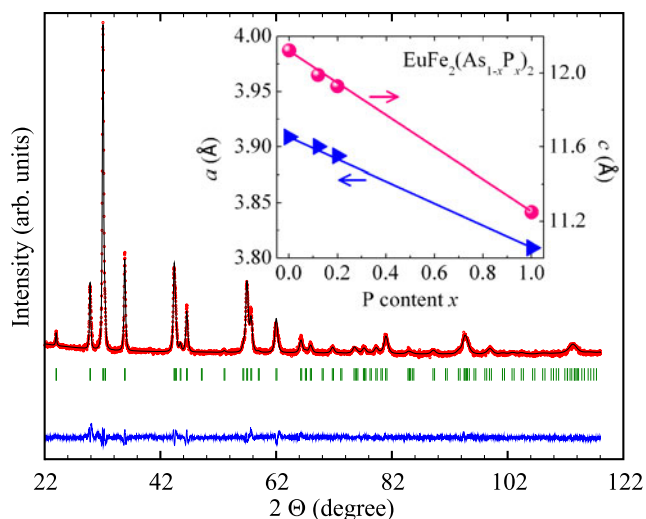


Fig. 1 X-ray powder diffraction pattern at room temperature for the sample $\text{EuFe}_2(\text{As}_{0.88}\text{P}_{0.12})_2$. The solid line represents a Rietveld refinement profile. The residuals are plotted at the bottom of the figure. In the inset, refined lattice parameters are plotted as a function of P content x

structure. An example of the refinement profile for $\text{EuFe}_2(\text{As}_{0.88}\text{P}_{0.12})_2$ is shown in Fig. 1. No obvious secondary phase can be detected. The weighted pattern factor and goodness of fit are $R_{\text{wp}} \sim 11.2\%$ and $S \sim 1.6$, respectively, indicating a fairly good refinement. In addition, the refined occupancies are close to the nominal values. The lattice constants for the tetragonal unit cell based upon the Rietveld refinements are $a = 3.9095(2)$ Å and $c = 11.979(1)$ Å for $x = 0.12$, $a = 3.9006(2)$ Å and $c = 11.9312(1)$ Å for $x = 0.2$, $a = 3.8152(2)$ Å and $c = 11.2401(1)$ Å for $x = 1$. The values for $x = 1$ are in agreement with the literature values [$a = 3.8178(1)$ Å and $c = 11.2372(3)$ Å] [25]. The lattice constants a and c as a function of x are plotted in the inset of Fig. 1. A decrease of both a and c with increasing x is observed. The decrease of the lattice constant c as a result of P substitution implies an increase of the coupling between the Eu and the $\text{Fe}_2(\text{As}_{1-x}\text{P}_x)_2$ layers. This might also be important for the evolution of the magnetic order in the Eu-sublattice, since the Ruderman–Kittel–Kasuya–Yosida (RKKY) coupling strongly depends on the distance between the magnetic ions [13, 18, 25].

3.1.2 Magnetization Measurements

The temperature dependence of the zero-field-cooled (ZFC) and field-cooled (FC) magnetic susceptibility $\chi = M/H$ for $\text{EuFe}_2(\text{As}_{1-x}\text{P}_x)_2$ ($x = 0.12, 0.2$, and 1) in a magnetic field of $\mu_0 H = 2$ mT is shown in Fig. 2. The results for $x = 0$ were already discussed in detail in our previous work [21], and hence, are not shown here. The magnetic susceptibility at high temperatures (i.e., far above the magnetic ordering temperature of the Eu^{2+} moments T_{Eu}) is well described by

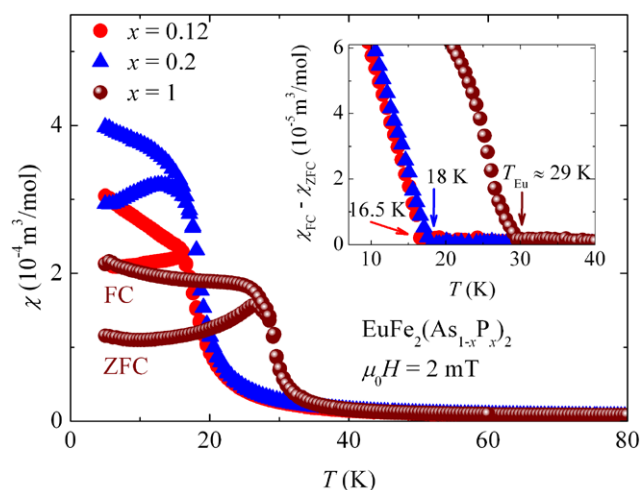


Fig. 2 Temperature dependence of the ZFC and FC magnetic susceptibility for the samples $\text{EuFe}_2(\text{As}_{1-x}\text{P}_x)_2$ ($x = 0.12, 0.2, 1$) measured in a magnetic field of $\mu_0 H = 2$ mT. The inset illustrates the temperature dependence of the difference of both susceptibilities ($\chi_{\text{FC}} - \chi_{\text{ZFC}}$). The arrows mark the magnetic ordering temperatures T_{Eu} of the Eu^{2+} moments

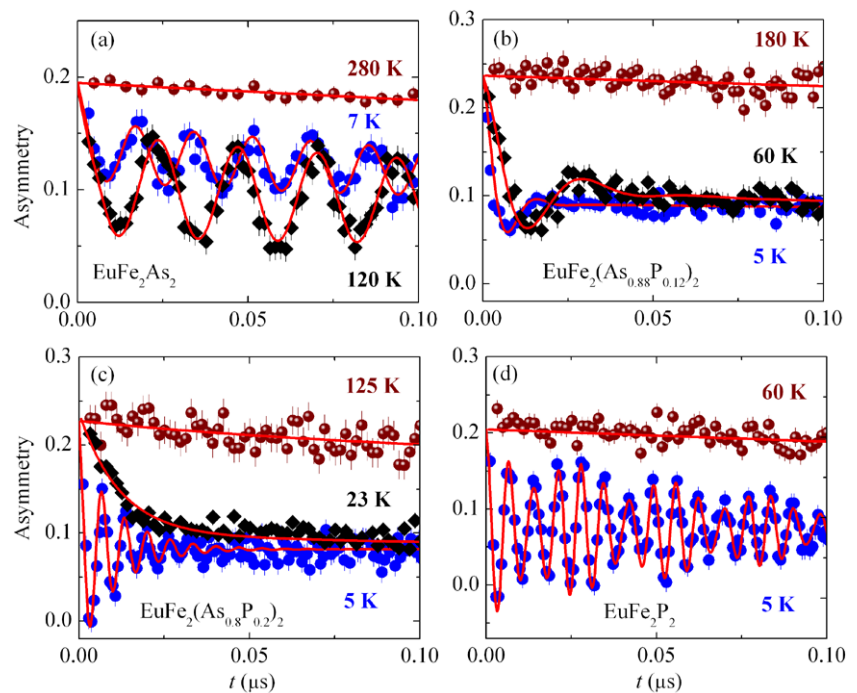
the Curie–Weiss law:

$$\chi(T) = \frac{C}{T - \theta_{\text{CW}}}. \quad (1)$$

Here, C denotes the Curie constant and θ_{CW} the paramagnetic Curie–Weiss temperature. An analysis of the data in Fig. 2 with Eq. (1) yields: $\theta_{\text{CW}} = 16.74(8)$ K, $\mu_{\text{eff}} \simeq 8.1 \mu_B$ for $x = 0.12$, $\theta_{\text{CW}} = 18.14(7)$ K, $\mu_{\text{eff}} \simeq 8.2 \mu_B$ for $x = 0.2$, and $\theta_{\text{CW}} = 29.35(9)$ K, $\mu_{\text{eff}} \simeq 8.3 \mu_B$ for $x = 1$. The obtained values of μ_{eff} are close to the theoretical value of a free Eu^{2+} ion ($\mu_{\text{Eu}^{2+}} = 7.94 \mu_B$).

As shown in Fig. 2, for all the P substituted samples an obvious deviation between χ_{ZFC} and χ_{FC} is seen at low temperatures. This is not the case for $x = 0$ [18, 21], for which AFM order of Eu^{2+} with the moments pointing along the a axis was reported. This result is consistent with previous magnetization studies [26], suggesting that the ground state of the coupled Eu^{2+} spins is a canted AFM state (C-AFM state) (i.e., AFM with the net ferromagnetic (FM) component along the c -axis) in $\text{EuFe}_2(\text{As}_{1-x}\text{P}_x)_2$ ($x = 0.12, 0.2$) and a FM state in EuFe_2P_2 . Recently, neutron diffraction measurements were also performed on EuFe_2P_2 and an almost axial FM structure of the Eu^{2+} spins was established [27]. The C-AFM and FM structure of the Eu-sublattice in $\text{EuFe}_2(\text{As}_{1-x}\text{P}_x)_2$ ($x = 0.12, 0.2, 1$) sharply contrasts with the planar antiferromagnetism seen in the parent compound EuFe_2As_2 , suggesting a delicate interplay between the Eu $4f$ and the Fe $3d$ electrons. It was concluded from different experiments [12, 13] that there is a strong coupling between the localized Eu^{2+} spins and the conduction electrons of the two-dimensional (2D) Fe_2As_2 layers in EuFe_2As_2 . This revealed that the magnetic exchange interaction between the

Fig. 3 ZF μ SR spectra for $\text{EuFe}_2(\text{As}_{1-x}\text{P}_x)_2$ ($x = 0, 0.12, 0.2, 1$) recorded for three different temperatures: $T < T_{\text{Eu}}$ (circles), $T_{\text{Eu}} < T < T_{\text{SDW}}$ (diamonds), and $T > T_{\text{SDW}}$ (spheres). The solid lines represent fits to the data by means of Eq. (2)



localized Eu $4f$ moments is mediated by the itinerant Fe $3d$ electrons. However, the interaction of the Eu moments with the magnetic moments of the Fe sublattice (band magnetism) cannot be neglected. Only a combination of both interactions can further elucidate the C-AFM ground state observed in $\text{EuFe}_2(\text{As}_{1-x}\text{P}_x)_2$ ($x = 0.12$ and 0.2). Note that a C-AFM ground state was also found in the related compound $\text{EuFe}_{1.8}\text{Co}_{0.2}\text{As}_2$ [21].

The magnetic ordering temperature T_{Eu} of the Eu^{2+} moments was determined by the temperature at which the difference between χ_{ZFC} and χ_{FC} sets in (see the inset of Fig. 2). It was found to be $T_{\text{Eu}} \simeq 16.5, 18$, and 29 K for $x = 0.12, x = 0.2$, and $x = 1$, respectively. The value of T_{Eu} for $x = 0.12$ is slightly reduced compared to $T_{\text{Eu}} \simeq 19$ K for the parent compound $x = 0$. However, on further increasing the P concentration T_{Eu} increases and reaches a maximum for $x = 1$. The value of T_{Eu} for $x = 1$ is in agreement with those reported in literature [19, 25, 27].

3.1.3 Zero-Field μ SR Measurements

In a μ SR experiment, nearly 100 % spin-polarized muons μ^+ are implanted into the sample one at a time. The positively charged μ^+ thermalize at interstitial lattice sites, where they act as magnetic microprobes. In a magnetic material, the muon spin precesses in the local magnetic field B_μ at the muon site with the Larmor frequency $\nu_\mu = \gamma_\mu/(2\pi)B_\mu$ (muon gyromagnetic ratio $\gamma_\mu/(2\pi) = 135.5 \text{ MHz T}^{-1}$). ZF μ SR is a very powerful tool to investigate microscopic magnetic properties of solids without applying an external magnetic field.

ZF μ SR time spectra for the single crystal of EuFe_2As_2 and for the polycrystalline samples $\text{EuFe}_2(\text{As}_{1-x}\text{P}_x)_2$ are shown in Fig. 3, recorded for three different temperatures: $T < T_{\text{Eu}}$, $T_{\text{Eu}} < T < T_{\text{SDW}}$, and $T > T_{\text{SDW}}$. For EuFe_2As_2 , the ZF μ SR measurements were performed with the initial muon spin polarization tilted by approximately 45° away from the crystallographic c -axis. At high temperatures (see Fig. 3), no muon spin precession and only a very weak depolarization of the μ SR signal is observed. This weak depolarization and its Gaussian functional form are typical for a paramagnetic material and reflect the occurrence of a small Gaussian–Kubo–Toyabe depolarization, originating from the interaction of the muon spin with randomly oriented nuclear magnetic moments. At temperatures below T_{Eu} a well-defined spontaneous muon spin precession is observed in all compounds, indicating long-range magnetic order of the Eu^{2+} moments in the investigated compounds. For $x = 0$ and 0.12 above $T_{\text{Eu}} \simeq 20.5$ and 16.5 K, respectively, muon spin precession with a lower frequency is observed which is caused by the long-range SDW order of the Fe moments. However, for $x = 0.2$, instead of the oscillatory behavior seen in the SDW state for $x = 0$ and 0.12 , a fast decaying signal is observed (see Fig. 3(c)). The reason for this strongly decaying μ SR signal will be discussed below. For $x = 1$, only the magnetic ordering of the Eu moments is seen in the μ SR spectra (Fig. 3(d)). Note that for $x = 0, 0.12$ and 0.2 only one μ SR frequency is visible. However, for $x = 1$ two distinct precession frequencies occur in the μ SR spectra, corresponding to the local magnetic fields $B_{\mu,\text{Eu}}^1 \simeq 1.08 \text{ T}$ ($\simeq 70\%$ of the signal) and $B_{\mu,\text{Eu}}^2 \simeq 1.37 \text{ T}$

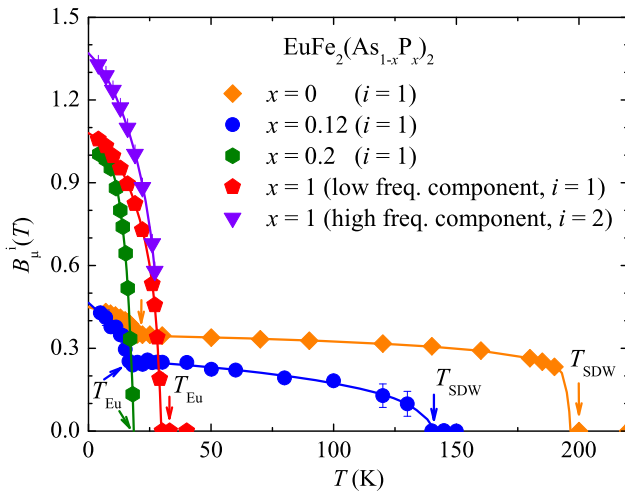


Fig. 4 The temperature dependence of the internal magnetic field B_{μ}^i for the samples $\text{EuFe}_2(\text{As}_{1-x}\text{P}_x)_2$ ($x = 0, 0.12, 0.2$, and 1). The solid lines represent fits to the data by means of Eq. (3). The arrows mark the transition temperatures for the SDW (T_{SDW}) and the Eu magnetic order (T_{Eu})

($\approx 30\%$ of the signal). This indicates that two magnetically inequivalent muon stopping sites are present in EuFe_2P_2 .

The ZF μSR data were analyzed using the following functional form:

$$A(t) = \sum_{i=1}^2 A_0^i [\alpha_i e^{-\lambda_T^i t} \cos(\gamma_{\mu} B_{\mu}^i t + \varphi) + \beta_i e^{-\lambda_L^i t}]. \quad (2)$$

α_i and $\beta_i = 1 - \alpha_i$ ($i = 1$ for $x = 0, 0.12, 0.2$, and $i = 1, 2$ for $x = 1$) are the fractions of the oscillating and nonoscillating μSR signal. For the single crystal ($x = 0$) one finds $\alpha_1 = 0.73(2)$ and $\beta_1 = 0.27(3)$. However, for the polycrystalline samples $\alpha_i = 2/3$ and $\beta_i = 1/3$. The $2/3$ oscillating and the $1/3$ nonoscillating μSR signal fractions originate from the spatial averaging in powder samples where only $2/3$ of the magnetic field components are perpendicular to the muon spin and cause muon spin precession. A_0 denotes the initial asymmetry, and φ is the initial phase of the muon-spin ensemble. B_{μ}^i represents the internal magnetic field at the muon site, and the depolarization rates λ_T^i and λ_L^i characterize the damping of the oscillating and nonoscillating part of the μSR signal, respectively. The transversal relaxation rate λ_T^i is a measure of the width of the static magnetic field distribution at the muon site, and also reflects dynamical effects (spin fluctuations). The longitudinal relaxation rate λ_L^i is determined by dynamic magnetic fluctuations only [28]. The temperature dependence of the internal magnetic field B_{μ}^i for $\text{EuFe}_2(\text{As}_{1-x}\text{P}_x)_2$ is shown in Fig. 4. B_{μ}^i is proportional to the magnitude of the ordered moment and thus to the magnetic order parameter. The second component ($i = 2$) in the μSR signal was observed only for $x = 1$, and hence, we will discuss the x -dependence of

the relevant physical parameters related to the first component ($i = 1$) only. For $x = 0$ a sharp step like increase of B_{μ}^1 is observed below ≈ 195 K, which reflects the appearance of the SDW ordering of the Fe moments. The value of T_{SDW} is in good agreement with $T_{\text{SDW}} \approx 190$ K obtained from neutron diffraction [11]. A sharp increase of B_{μ}^1 is an indication for a first order transition. A first order transition due to SDW formation was also observed in the related compound SrFe_2As_2 [29]. Upon lowering the temperature B_{μ}^1 first tends to saturate, but increases again when the magnetic order of the Eu^{2+} moments occurs at T_{Eu} . To describe the temperature dependence of B_{μ}^i , we assumed the following phenomenological function:

$$\bar{B}_{\mu}^i(T) = \bar{B}_{\mu,\text{Eu}}^i(0) \left[1 - \left(\frac{T}{T_{\text{Eu}}} \right)^{\gamma_1} \right]^{\delta_1} + \bar{B}_{\mu,\text{SDW}}^i(0) \left[1 - \left(\frac{T}{T_{\text{SDW}}} \right)^{\gamma_2} \right]^{\delta_2}, \quad (3)$$

where $B_{\mu,\text{Eu}}^i(0)$ and $B_{\mu,\text{SDW}}^i(0)$ represent the zero-temperature values of the internal magnetic field probed by the muons in the Eu and in the SDW ordered states, respectively. γ and δ are empirical exponents. As indicated by the solid lines in Fig. 4 the function in Eq. (3) describes the data reasonably well, yielding the parameters given in Table 1. Note that with increasing x the values of T_{SDW} and $B_{\mu,\text{SDW}}^1(0)$ decrease, and for $x = 0.2$ and $x = 1$ no long-range SDW order of the Fe moments is observed. On the other hand, T_{Eu} decreases with increasing x , reaches minimum at $x = 0.12$ and then increases again, in agreement with the above susceptibility measurements. In addition, $B_{\mu,\text{Eu}}^1(0)$ significantly increases with x above $x = 0.12$. Considering the magnetization results, the increase of $B_{\mu,\text{Eu}}^1(0)$ may be ascribed to the appearance/growth of the ferromagnetic component as a result of P substitution. However, without microscopic modeling (i.e., calculation of the μ stopping site and the dipolar fields at the μ site) it is not possible to conclude how a change of the magnetic structure with P substitution would affect the internal field at the muon site.

The temperature dependences of the transverse and longitudinal depolarization rates λ_T^1 and λ_L^1 are presented in Fig. 5(a) and (b), respectively. Note that λ_T^1 is much smaller for the end members $x = 0, 1$ of the investigated system than for the mixed compounds $x = 0.12, 0.2$. As shown in Fig. 5(a), for $x = 0, 0.12$, and 0.2 , the onset of the Fe magnetic order is accompanied by an increase of λ_T^1 that decreases with decreasing temperature. Upon reaching the magnetic ordering temperature of Eu λ_T^1 shows another maximum. For $x = 1$, the strong increase of λ_T^1 around T_{Eu} is only due the Eu order. No SDW transition is observed at higher temperatures. The magnetic ordering temperatures of Eu (T_{Eu}) and Fe (T_{SDW}) are also clearly visible in the longitudinal relaxation rate λ_L^1 , which also shows a clear anomaly

Table 1 Summary of the parameters obtained for the polycrystalline samples of $\text{EuFe}_2(\text{As}_{1-x}\text{P}_x)_2$ ($x = 0, 0.12, 0.2, 1$) by means of magnetization and μSR experiments. T_{Eu}^{χ} and $T_{\text{Eu}}^{\mu\text{SR}}$ are the magnetic ordering temperatures of the Eu moments determined by susceptibility and μSR measurements. T_{SDW} denotes the SDW ordering temperature

x	T_{Eu}^{χ} (K)	$T_{\text{Eu}}^{\mu\text{SR}}$ (K)	T_{SDW} (K)	$B_{\mu,\text{Eu}}^1(0)$ (T)	$B_{\mu,\text{Eu}}^2(0)$ (T)	$B_{\mu,\text{SDW}}^1(0)$ (T)	$B_{\mu,\text{SDW}}^2(0)$ (T)
0	19.5(6)	20.5(5)	195(3)	0.45(1)	—	0.35(1)	—
0.12	16.5(5)	16.7(6)	140(5)	0.476(12)	—	0.258(10)	—
0.2	17.9(5)	18.4(2)	85	0.997(12)	—	0	—
1	29.5(5)	29.3(4)	0	1.08(1)	1.37(2)	0	0

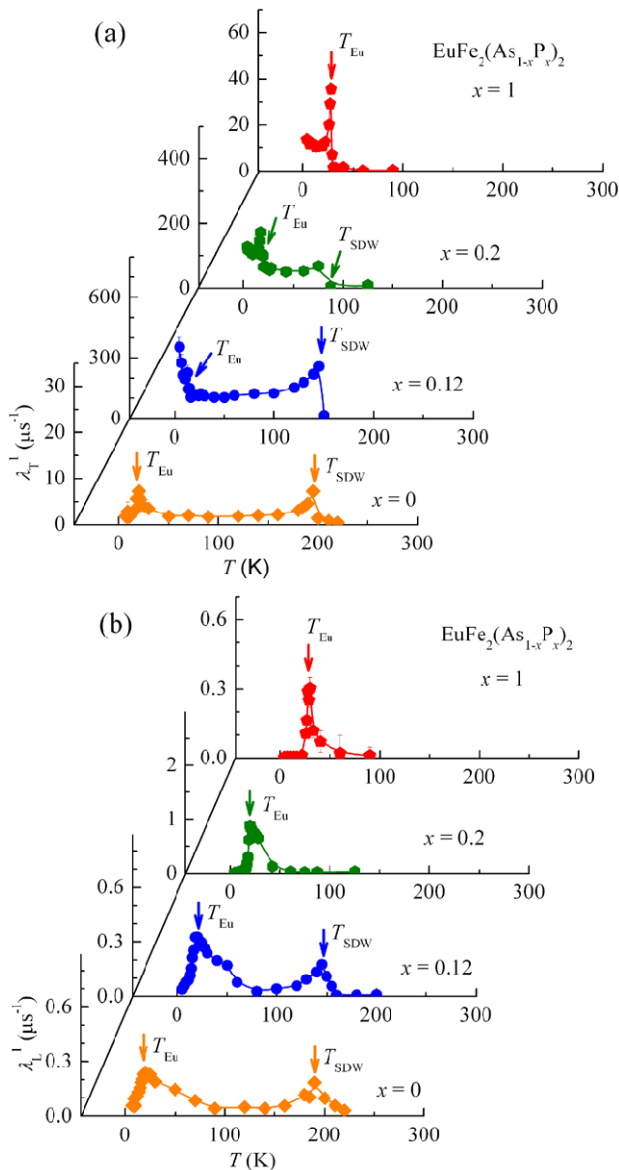


Fig. 5 (a) Transverse relaxation rate λ_T^1 (T) for the samples $\text{EuFe}_2(\text{As}_{1-x}\text{P}_x)_2$ with $x = 0, 0.12, 0.2$, and 1. Lines are guides to the eye. (b) Longitudinal relaxation rate λ_L^1 (T) for $\text{EuFe}_2(\text{As}_{1-x}\text{P}_x)_2$ ($x = 0, 0.12, 0.2, 1$). The arrows mark the transition temperatures for the high-temperature SDW (T_{SDW}) and the low-temperature Eu order (T_{Eu})

of the Fe moments determined from μSR experiments. $B_{\mu,\text{Eu}}^i(0)$ and $B_{\mu,\text{SDW}}^i(0)$ ($i = 1, 2$) represent the zero-temperature values of the internal magnetic fields at the muon site probed in the Eu and the SDW ordered state

at T_{Eu} and T_{SDW} (see Fig. 5(b)). As mentioned above, for the sample with $x = 0.2$ (see Fig. 3(c), diamonds) only a fast depolarization of the implanted muons is observed above T_{Eu} , but no coherent precession signal. The fast depolarization of the μSR signal could be either due to a wide distribution of static fields, and/or to strongly fluctuating magnetic moments. To discriminate between these two possibilities we compare the values of λ_T^1 and λ_L^1 . Note that for $x = 0.2$, and $T < 85$ K λ_T^1 is very large ($\simeq 50$ MHz) while λ_L^1 is small ($\simeq 0.05$ MHz). λ_T^1 consists of a static as well as of a dynamic contribution, while λ_L^1 contains only a dynamic contribution. Since in our case $\lambda_T^1 \gg \lambda_L^1$, the static contribution dominates λ_T^1 , and the fast depolarization of the μSR signal observed for $x = 0.2$ is due to the (quasi)-static disordered SDW phase with $T_{\text{SDW}} \simeq 85$ K. The important parameters for all samples extracted from the magnetization and the μSR experiments are summarized in Table 1.

Very recently, bulk superconductivity with $T_c \simeq 28$ K was reported in single crystals of P substituted $\text{EuFe}_2(\text{As}_{1-x}\text{P}_x)_2$ [19] based on resistivity, magnetization, and specific heat measurements. However, superconductivity coexisting with AFM Eu^{2+} order was only found in a very narrow x range ($0.16 \leq x \leq 0.22$), where the SDW transition is suppressed. In the present study, no indication of superconductivity was seen for $x = 0.2$ from magnetization measurements. This might be due to the fact that in our sample ($x = 0.2$) the SDW state is not completely suppressed as supported by the μSR measurements. In addition to chemical pressure, the physical properties of EuFe_2As_2 can be also tuned by the application of hydrostatic pressure [6, 20]. Previous reports of high pressure experiments on EuFe_2As_2 revealed pressure-induced superconductivity in a narrow pressure range of 2.5–3.0 GPa [6, 20], accompanied by a suppression of the SDW state of the Fe moments. Since pressure experiments on EuFe_2As_2 were already reported by various groups [6, 20], we decided to study pressure effects in the P substituted sample $\text{EuFe}_2(\text{As}_{0.88}\text{P}_{0.12})_2$. The sample with $x = 0.12$ was chosen for the following reasons: (i) According to the SC phase diagram reported [19] for EuFe_2As_2 as a function of chemical pressure (P con-

tent x), the sample with $x = 0.12$ is close to the value of x at which superconductivity appears. By applying hydrostatic pressure, the SC phase might be reachable. (ii) Based on previous reports [6, 20], superconductivity was found in the vicinity of the pressure value where the SDW state is suppressed.

In the following sections, the results of the magnetization and the μ SR experiments performed on $\text{EuFe}_2(\text{As}_{0.88}\text{P}_{0.12})_2$ under hydrostatic pressures are presented.

3.2 Hydrostatic Pressure Effect on $\text{EuFe}_2(\text{As}_{0.88}\text{P}_{0.12})_2$

3.2.1 High Pressure Magnetization Measurements

Magnetization measurements were carried out under hydrostatic pressures up to $p = 5.9$ GPa. The temperature dependence of the ZFC and FC magnetic susceptibilities χ for $\text{EuFe}_2(\text{As}_{0.88}\text{P}_{0.12})_2$ recorded at ambient and selected applied pressures is shown in Fig. 6(a) ($p \leq 0.4$ GPa), in Fig. 6(b) (0.42 GPa $\leq p \leq 0.55$ GPa), and in Fig. 6(c) (1.1 GPa $\leq p \leq 5.9$ GPa). Note that Fig. 6 shows the data after subtraction of the background signal from the empty pressure cell. The magnetic ordering temperature T_{Eu} of the Eu^{2+} moments was determined as described in Sect. 3.1.2. At ambient pressure, a clear bifurcation between the ZFC and FC curves appears below $T_{\text{Eu}} \simeq 16.5$ K, which is consistent with the susceptibility data obtained for the sample without pressure cell (see Fig. 2). In addition, the magnitudes of the susceptibilities are also in fair agreement. Upon increasing the pressure, an anomaly in the ZFC susceptibility is observed at $p = 0.4$, 0.42 , and 0.48 GPa as shown in Fig. 6(a) and (b). The low-temperature data for $p = 0.4$ GPa are shown in the inset of Fig. 6(a). In addition to the Eu order observed at $\simeq 18$ K, a strong decrease of the ZFC susceptibility is observed at $\simeq 11$ K, which is possibly due to the appearance of superconductivity. The decrease of the susceptibility corresponds to nearly 100 % diamagnetic shielding. In order to confirm superconductivity, transport measurements under pressure are necessary. Just magnetization data do not allow to conclude that the observed decrease of χ_{ZFC} is due to the appearance of superconductivity. Hence we call this phase “X”. For $p = 0.42$ GPa, the susceptibility also shows a pronounced decrease at $T_{\text{X}} \simeq 20$ K (see Fig. 2(b), the low-temperature data are shown in the inset). Below $\simeq 18.2$ K, the susceptibility starts to increase again due to the C-AFM ordering of the Eu^{2+} moments. Upon increasing the pressure to $p = 0.47$ GPa, the transition temperature T_{X} decreases to 8.8 K. Above $p = 0.55$ GPa, the “X” phase is no longer visible (see Fig. 6(c)). It is also absent for $p < 0.35$ GPa. Therefore, pressure-induced “X” phase in $\text{EuFe}_2(\text{As}_{0.88}\text{P}_{0.12})_2$ is very likely present in a very narrow pressure range. We observed that T_{Eu} increases upon

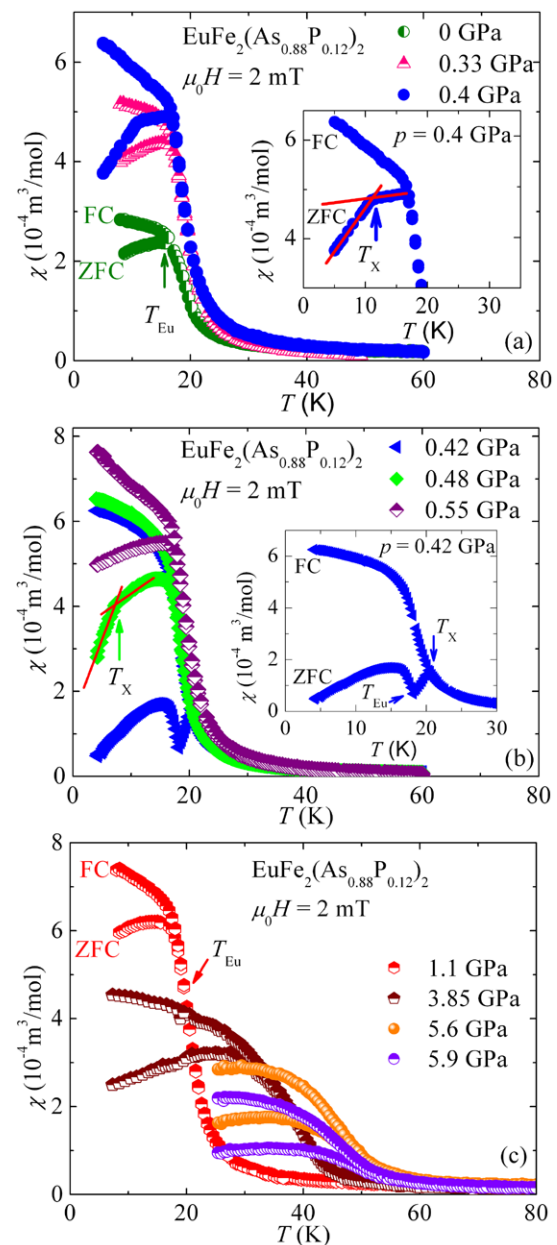
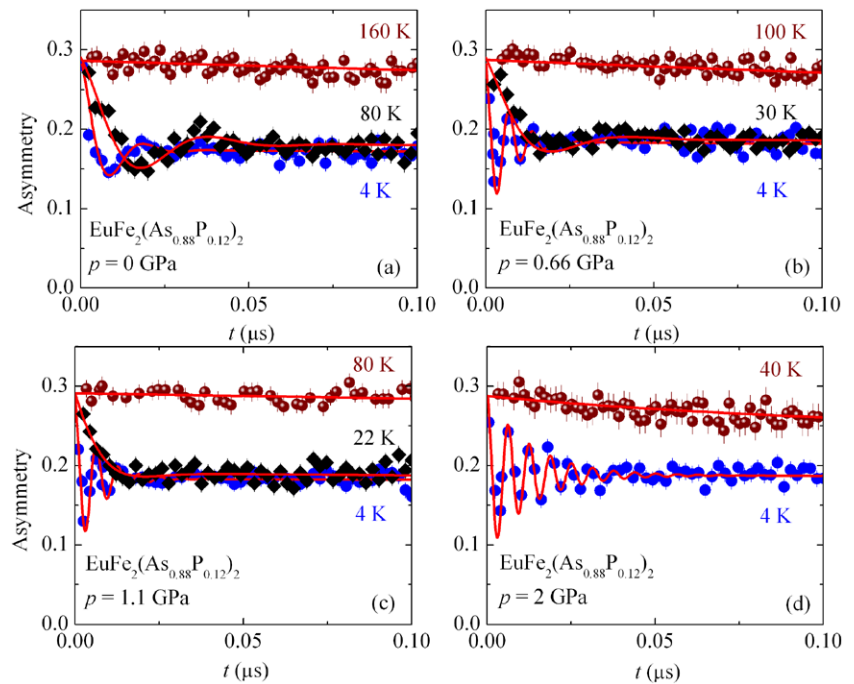


Fig. 6 Temperature dependence of the ZFC and FC magnetic susceptibility of $\text{EuFe}_2(\text{As}_{0.88}\text{P}_{0.12})_2$ in a magnetic field of $\mu_0 H = 2$ mT for $p \leq 0.4$ GPa (a), for 0.42 GPa $\leq p \leq 0.55$ GPa (b), and for 1.1 GPa $\leq p \leq 5.9$ GPa (c). The arrows mark the ordering temperature of Eu moments (T_{Eu}) and the “X” transition temperatures (T_{X}). The insets of panels (a) and (b) show the low temperature data for $p = 0.4$ GPa and 0.42 GPa, respectively, illustrating the transition to the superconducting state marked by the arrows. The solid lines are guides to the eye

increasing hydrostatic pressure, similar to chemical pressure. The maximum value of $T_{\text{Eu}} = 56$ K is reached at $p = 5.6$ GPa, and at higher pressures it tends to decrease (see Fig. 6(c)). For instance, $T_{\text{Eu}} = 53$ K at the maximum applied pressure $p = 5.9$ GPa. A maximum of T_{Eu} was also

Fig. 7 ZF μ SR spectra of $\text{EuFe}_2(\text{As}_{0.88}\text{P}_{0.12})_2$ measured at $p = 0.0, 0.66, 1.1$, and 2 GPa, recorded for three different temperatures: $T < T_{\text{Eu}}$ (circles), $T_{\text{Eu}} < T < T_{\text{SDW}}$ (diamonds), and $T > T_{\text{SDW}}$ (spheres). The solid lines represent fits to the data by means of Eq. (4)



observed for the parent compound EuFe_2As_2 , but at higher pressure ($p = 8$ GPa). According to recent X-ray diffraction studies [30] of EuFe_2As_2 , a collapsed tetragonal (cT) phase was found above 8 GPa. It is known that the pressure-induced structural transition toward the cT phase is connected with a valence change of the Eu ions, as reported for EuFe_2P_2 and EuCo_2P_2 [31]. Therefore, it is possible that the decrease of T_{Eu} above 5.6 GPa is connected with a pressure-induced valence change from the magnetic Eu^{2+} to the non-magnetic Eu^{3+} state. However, to gain further insight into this pressure region, measurements at $p > 5.9$ GPa are necessary.

3.2.2 Zero-Field μ SR Measurements Under Pressure

Hydrostatic pressure effects on the magnetic properties of $\text{EuFe}_2(\text{As}_{0.88}\text{P}_{0.12})_2$ were studied microscopically by means of ZF μ SR. Some representative μ SR time spectra at different applied pressures are shown in Fig. 7. A substantial fraction of the μ SR asymmetry signal originates from muons stopping in the MP35N pressure cell [23] surrounding the sample. Therefore, the total μ SR asymmetry is a sum of two components:

$$A^{\text{ZF}}(t) = A_{\text{S}}^{\text{ZF}}(t) + A_{\text{PC}}^{\text{ZF}}(t), \quad (4)$$

$A_{\text{S}}^{\text{ZF}}(t)$ is the contribution of the sample, and $A_{\text{PC}}^{\text{ZF}}(t)$ is the contribution of the pressure cell. $A_{\text{S}}^{\text{ZF}}(t)$ is well described

by Eq. (2) with $\alpha_1 = 2/3$ and $\beta_1 = 1/3$ (since for $x = 0.12$ the μ SR spectra contain only one frequency, $\alpha_2 = 0$ and $\beta_2 = 0$). The signal of the pressure cell was analyzed by a damped Kubo–Toyabe (KT) function [23]:

$$A_{\text{PC}}^{\text{ZF}}(t) = A_{\text{PC}}^{\text{ZF}}(0) \left[\frac{1}{3} + \frac{2}{3}(1 - \sigma t)e^{-\sigma^2 t^2/2} \right] e^{-\lambda t}. \quad (5)$$

Here $A_{\text{PC}}^{\text{ZF}}(0)$ is the amplitude of $A_{\text{PC}}^{\text{ZF}}(t)$ at $t = 0$. The width of the static Gaussian field distribution $\sigma = 0.338 \mu\text{s}^{-1}$ and the damping rate $\lambda = 0.04 \mu\text{s}^{-1}$ were obtained from a measurement of the empty pressure cell. The total initial asymmetry is $A_{\text{S}}^{\text{ZF}}(0) + A_{\text{PC}}^{\text{ZF}}(0) = 0.29$. The ratio $A_{\text{S}}^{\text{ZF}}(0)/[A_{\text{S}}^{\text{ZF}}(0) + A_{\text{PC}}^{\text{ZF}}(0)] \simeq 40\%$ implies that approximately 40 % of the muons are stopping in the sample. Up to $p = 1.1$ GPa the spontaneous muon-spin precession in the Eu ordered and in the SDW state is clearly observed in the ZF μ SR time spectra (see Fig. 7), indicating long range magnetic order in the Eu and the Fe sublattice. Above $p = 1.1$ GPa the SDW state is suppressed and only the magnetic order of the Eu moments remains. The temperature dependence of the internal field B_{μ}^1 for various hydrostatic pressures is shown in Fig. 8. The inset shows $B_{\mu,\text{Eu}}^1$ at low temperatures where the magnetic ordering of the Eu^{2+} moments is evident. The data were analyzed by Eq. (3). The SDW ordering temperature T_{SDW} of the Fe moments ($T_{\text{SDW}} = 140$ K at ambient pressure) as well as $B_{\mu,\text{SDW}}^1$ created by the Fe sublattice decrease with increasing pressure. Above $p = 1.1$ GPa, the SDW order is completely suppressed. On the contrary, T_{Eu} increases with pressure,

in agreement with the susceptibility measurements. In addition, $B_{\mu,\text{Eu}}^1$ related to the Eu ordered state also increases with pressure. Note the sharp increase of $B_{\mu,\text{Eu}}^1$ below T_{Eu} with increasing the pressure from $p = 0$ GPa to $p = 0.44$ GPa. For $p > 0.44$ GPa, a more smooth increase of $B_{\mu,\text{Eu}}^1$ is observed. Relevant parameters of $\text{EuFe}_2(\text{As}_{0.88}\text{P}_{0.12})_2$ extracted from the high pressure magnetization and μSR experiments are listed in Table 2.

As shown above the magnetization measurements indicate the presence of a possible SC phase in the pressure

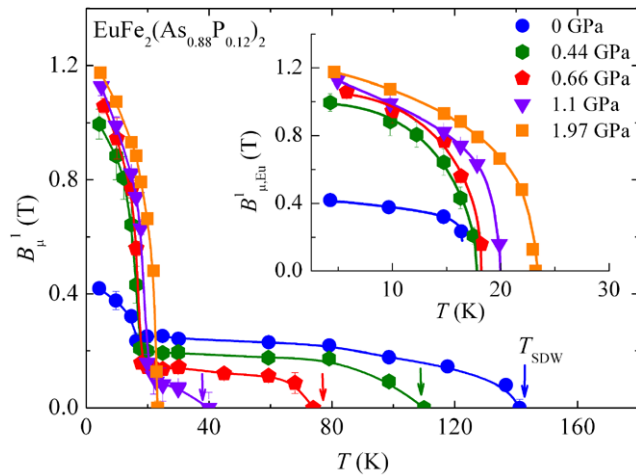


Fig. 8 Temperature dependence of the internal field B_{μ}^1 at the muon site for the sample $\text{EuFe}_2(\text{As}_{0.88}\text{P}_{0.12})_2$ recorded at various applied pressures. The solid lines represent fits to the data by means of Eq. (3). The arrows mark the ordering temperature T_{SDW} . The inset shows the low temperature data, illustrating the transition at T_{Eu} to the magnetically ordered state of the Eu moments

Table 2 Summary of the parameters obtained for the polycrystalline sample of $\text{EuFe}_2(\text{As}_{0.88}\text{P}_{0.12})_2$ at different hydrostatic pressures by means of magnetization and μSR experiments. The meaning of the symbols is given in the text

p (GPa)	T_{Eu}^{χ} (K)	$T_{\text{Eu}}^{\mu\text{SR}}$ (K)	T_{X} (K)	$T_{\text{SDW}}^{\mu\text{SR}}$ (K)	$B_{\mu,\text{Eu}}^1(0)$ (T)	$B_{\mu,\text{SDW}}^1(0)$ (T)
0	16.5(5)	16.4(3)	–	141.2(1)	0.44(1)	0.25(1)
0.4	17.5(4)	–	11.2(3)	–	–	–
0.42	17.6(5)	–	20.3(3)	–	–	–
0.44	–	17.7(3)	–	110(1)	0.99(2)	0.19(2)
0.48	17.9(4)	–	7.3(3)	–	–	–
0.66	18.9(5)	18.4(6)	0	75(2)	1.07(5)	0.17(4)
1.1	20.5(5)	19.9(7)	0	40(3)	1.27(3)	0.12(2)
1.73	24.6(3)	–	0	–	–	–
1.97	24.4(5)	23.6(7)	0	0	1.23(2)	0
2.5	27.2(3)	–	0	–	–	–
3.85	35.8(5)	–	0	–	–	–
4.54	42.5(4)	–	0	–	–	–
5.1	49.5(3)	–	0	–	–	–
5.6	57(4)	–	0	–	–	–
5.9	53(5)	–	0	–	–	–

range $0.36 \text{ GPa} \leq p \leq 0.5 \text{ GPa}$. An attempt to detect it in the sample $\text{EuFe}_2(\text{As}_{0.88}\text{P}_{0.12})_2$ with ZF and TF μSR , failed because of the strong intrinsic magnetism present in the sample.

4 Phase Diagram

Figure 9(a) shows the $(x-T)$ phase diagram for the system $\text{EuFe}_2(\text{As}_{1-x}\text{P}_x)_2$. The $(p-T)$ phase diagram of $\text{EuFe}_2(\text{As}_{0.88}\text{P}_{0.12})_2$ is plotted in Fig. 9(b). The data for T_{Eu} represented by the triangles in Fig. 9(a) are taken from [25]. In the $(x-T)$ phase diagram, three different phases were identified: a paramagnetic phase (PM), spin-density wave order of the Fe moments (SDW), and magnetic order of Eu^{2+} moments (MO). Moreover, in the $(p-T)$ phase diagram, pressure-induced “X” phase was found (see the inset of Fig. 9(b)). In Fig. 10, the internal magnetic fields $B_{\mu,\text{Eu}}^1$ and $B_{\mu,\text{SDW}}^1$ probed by the muons in the Eu ordered and in the SDW state and the low temperature value of the magnetic susceptibility $\chi_{\text{ZFC}}(7 \text{ K})$ are plotted as a function of P content x and applied pressure p .

By combining the above phase diagrams, one obtains a coherent physical picture on the system EuFe_2As_2 upon P substitution and on $\text{EuFe}_2(\text{As}_{0.88}\text{P}_{0.12})_2$ under hydrostatic pressure. An important finding is the observation of pressure-induced “X” phase in $\text{EuFe}_2(\text{As}_{0.88}\text{P}_{0.12})_2$, coexisting with magnetic order of the Eu and Fe moments. “X” phase appears in the narrow pressure region of 0.36–0.5 GPa. The presented phase diagrams in combination with the results obtained for the parent compound under pressure [6, 20] allow us to draw the following conclusion on

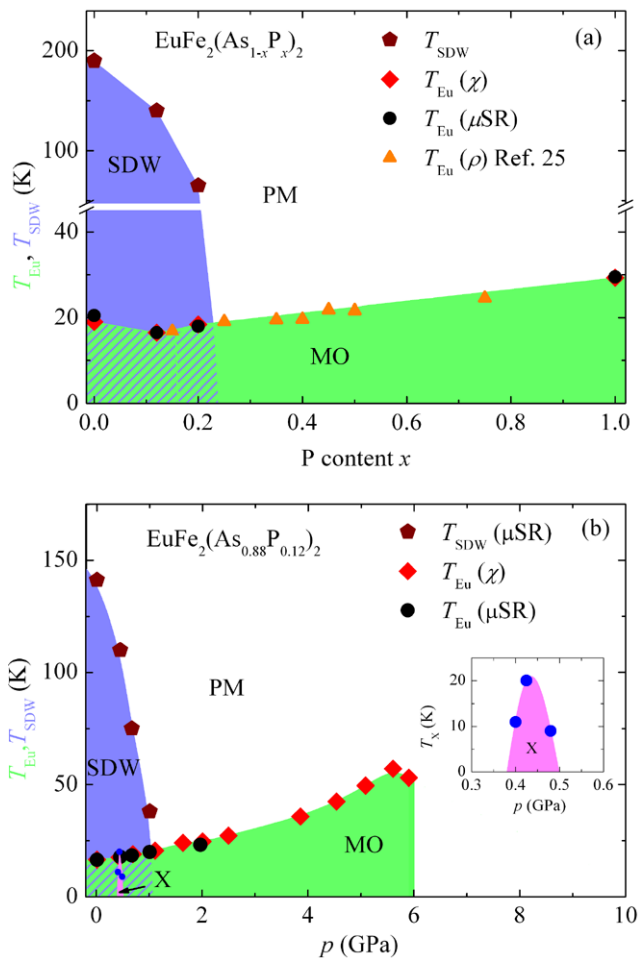


Fig. 9 (a) $(x-T)$ phase diagram of $\text{EuFe}_2(\text{As}_{1-x}\text{P}_x)_2$. The data points represented by the triangles are taken from [25]. (b) $(p-T)$ phase diagram of $\text{EuFe}_2(\text{As}_{0.88}\text{P}_{0.12})_2$. The various phases in the phase diagrams and the corresponding transition temperatures are denoted as follows: paramagnetic (PM), spin-density wave (SDW) and T_{SDW} , magnetic ordering of Eu (MO) and T_{Eu} , “X” phase (the meaning of this phase is given in the text) and T_X . For clarity, the inset in (b) shows the “X” phase present in a very narrow pressure range

the relation between chemical and hydrostatic pressure in EuFe_2As_2 :

- Both chemical and hydrostatic pressure suppress T_{SDW} and $B_{\mu, \text{SDW}}^1(0)$. However, the SDW ground state is differently affected by x and p . At all applied pressures below $p = 1.1$ GPa long-range SDW order was observed, while in the case of chemical pressure for $x = 0.2$ a disordered SDW phase exist. This may be related to the fact that by chemical pressure (P substitution) considerably more disorder is introduced.
- Figure 9 shows that in the case of P substitution T_{Eu} first decreases as a function of x , reaches a minimum at $x = 0.12$, and then increases. For a fixed P content of $x = 0.12$, the ordering temperature T_{Eu} increases with pressures up to $p = 5.6$ GPa. Above $p = 5.6$ GPa, how-

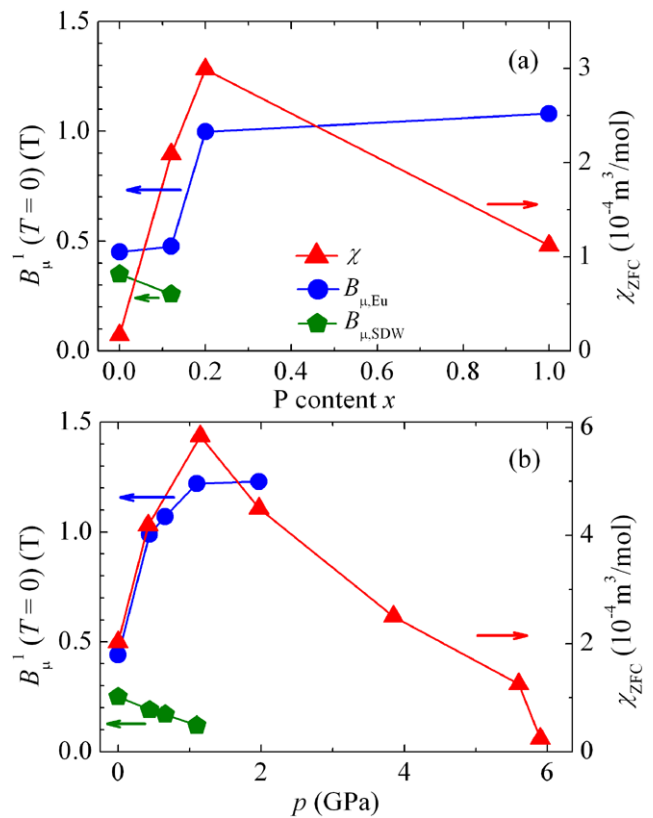


Fig. 10 Zero-temperature values of the internal magnetic fields $B_{\mu, \text{Eu}}^1$ and $B_{\mu, \text{SDW}}^1$ and the low-temperature value of the magnetic susceptibility χ_{ZFC} as a function of the P content x (a) and applied pressure (b)

ever, $T_{\text{Eu}}(p)$ decreases, accompanied by a possible valence change of the Eu moments. In the parent compound EuFe_2As_2 , a valence change was found at a higher pressure $p = 8$ GPa.

- The internal magnetic field $B_{\mu, \text{Eu}}^1(0)$ in the Eu ordered state increases with increasing x as well as by applying hydrostatic pressure (see Fig. 10(a)–(b)).
- The low temperature value of the magnetic susceptibility χ_{ZFC} (7 K) first increases with increasing x and p and above some critical values ($x = 0.2$ and $p = 1.1$ GPa) it decreases (see Fig. 10(a)–(b)).

By considering the findings listed above, the qualitative statement can be made that the properties of $\text{EuFe}_2(\text{As}_{1-x}\text{P}_x)_2$ are similarly tuned by chemical and hydrostatic pressure.

5 Conclusions

In summary, the magnetic and superconducting properties of the system $\text{EuFe}_2(\text{As}_{1-x}\text{P}_x)_2$ ($x = 0, 0.12, 0.2, 1$) were studied by magnetization and μSR experiments. In addition, the sample with $x = 0.12$ was also investigated by applying hydrostatic pressure up to $p \simeq 5.9$ GPa. The $(x-T)$ phase diagram of $\text{EuFe}_2(\text{As}_{1-x}\text{P}_x)_2$ and the $(p-T)$ phase diagram of

$\text{EuFe}_2(\text{As}_{0.88}\text{P}_{0.12})_2$ were determined and discussed as well as compared to the (p – T) phase diagram recently obtained for EuFe_2As_2 [6, 20]. The present investigations reveal that the magnetic coupling between the Eu and the Fe sublattices strongly depends on chemical and hydrostatic pressure and determines the (x – T) and (p – T) phase diagrams as presented in this work. According to the above discussed phase diagrams, chemical and hydrostatic pressures have qualitatively a similar effect on the Fe and Eu magnetic order.

There are still some open questions related to superconductivity and its interplay with the magnetic ground state of the system EuFe_2As_2 . One of the most interesting aspects of this particular member of Fe-based superconductors is the possibility to observe coexistence or competition between superconductivity and rare-earth Eu magnetic order. In the present work, the so-called “X” phase induced by pressure was observed in $\text{EuFe}_2(\text{As}_{0.88}\text{P}_{0.12})_2$ in addition to the magnetic phases of the Eu and Fe sublattices. It exists in a narrow pressure range 0.36–0.5 GPa. This phase is possibly superconducting. However, transport measurements as a function of pressure are required in order to clarify this point.

Acknowledgements This work was supported by the Swiss National Science Foundation, the SCOPES grant No. IZ73Z0_128242, and the NCCR Project MaNEP. The μ SR experiments were performed at the Swiss Muon Source of the Paul Scherrer Institute (PSI), Villigen, Switzerland.

References

- Kamihara, Y., Watanabe, T., Hirano, M., Hosono, H.: J. Am. Chem. Soc. **130**, 3296 (2008)
- Rotter, M., Tegel, M., Johrendt, D.: Phys. Rev. Lett. **101**, 107006 (2008)
- Chen, X.H., Wu, T., Wu, G., Liu, R.H., Chen, H., Fang, D.F.: Nature (London) **453**, 761 (2008)
- Torikachvili, M.S., Bud'ko, S.L., Ni, N., Canfield, P.C.: Phys. Rev. Lett. **101**, 057006 (2008)
- Fukazawa, H., Takeshita, N., Yamazaki, T., Kondo, K., Hirayama, K., Kohori, Y., Miyazawa, K., Kito, H., Eisaki, H., Iyo, A.: J. Phys. Soc. Jpn. **77**, 105004 (2008)
- Terashima, T., Kimata, M., Satsukawa, H., Harada, A., Hazama, K., Uji, S., Suzuki, H.S., Matsumoto, T., Murata, K.: J. Phys. Soc. Jpn. **78**, 083701 (2009)
- Ren, Z.A., Lu, W., Yang, J., Yi, W., Shen, X.L., Li, Z.C., Che, G.C., Dong, X.L., Sun, L.L., Zhou, F., Zhao, Z.X.: Chin. Phys. Lett. **25**, 2215 (2008)
- Matsuishi, S., Inoue, Y., Nomura, T., Hirano, M., Hosono, H.: J. Phys. Soc. Jpn. **77**, 113709 (2008)
- Zhao, J., Huang, Q., de la Cruz, C., Li, S., Lynn, J.W., Chen, Y., Green, M.A., Chen, G.F., Li, G., Li, Z., Luo, J.L., Wang, N.L., Dai, P.: Nat. Mater. **7**, 953 (2008)
- Raffius, H., Mörsen, M., Mosel, B.D., Müller-Warmuth, W., Jeitschko, W., Terbüchte, L., Vomhof, T.: J. Phys. Chem. Solids **54**, 135 (1993)
- Xiao, Y., Su, Y., Meven, M., Mittal, R., Kumar, C.M.N., Chatterji, T., Price, S., Persson, J., Kumar, N., Dhar, S.K., Thamizhavel, A., Brueckel, T.: Phys. Rev. B **80**, 174424 (2009)
- Jiang, S., Luo, Y.K., Ren, Z., Zhu, Z.W., Wang, C., Xu, X.F., Tao, Q., Cao, G.H., Xu, Z.A.: New J. Phys. **11**, 025007 (2009)
- Guguchia, Z., Roos, J., Shengelaya, A., Katrych, S., Bukowski, Z., Weyeneth, S., Murányi, F., Strässle, S., Maisuradze, A., Karpinski, J., Keller, H.: Phys. Rev. B **83**, 144516 (2011)
- Sefat, A.S., Jin, R., McGuire, M.A., Sales, B.C., Singh, D.J., Mandrus, D.: Phys. Rev. Lett. **101**, 117004 (2008)
- Leithe-Jasper, A., Schnelle, W., Geibel, C., Rosner, H.: Phys. Rev. Lett. **101**, 207004 (2008)
- He, Y., Wu, T., Wu, G., Zheng, Q.J., Liu, Y.Z., Chen, H., Ying, J.J., Liu, R.H., Wang, X.F., Xie, Y.L., Yan, Y.J., Dong, J.K., Li, S.Y., Chen, X.H.: J. Phys. Condens. Matter **22**, 235701 (2010)
- Li, L.J., Luo, Y.K., Wang, Q.B., Chen, H., Ren, Z., Tao, Q., Li, Y.K., Lin, X., He, M., Zhu, Z.W., Cao, G.H., Xu, Z.A.: New J. Phys. **11**, 025008 (2008)
- Ren, Z.: Phys. Rev. B **79**, 094426 (2009)
- Jeevan, H.S., Kasinathan, D., Rosner, H., Gegenwart, P.: Phys. Rev. B **83**, 054511 (2011)
- Matsubayashi, K., Munakata, K., Isobe, M., Katayama, N., Ohgushi, K., Ueda, Y., Uwatoko, Y., Kawamura, N., Mizumaki, M., Ishimatsu, N., Hedo, M., Umehara, I.: Phys. Rev. B **84**, 024502 (2011)
- Guguchia, Z., Bosma, S., Weyeneth, S., Shengelaya, A., Puzniak, R., Bukowski, Z., Karpinski, J., Keller, H.: Phys. Rev. B **84**, 144506 (2011)
- Rodríguez-Carvajal, J.: Physica B **192**, 55 (1993)
- Andreica, D.: Ph.D. Thesis, IPP/ETH-Zürich (2001)
- Suter, A., Wojek, B.M.: Phys. Procedia **30**, 69–73 (2012)
- Cao, G., Xu, S., Ren, Z., Jiang, S., Feng, C., Xu, Z.: J. Phys. Condens. Matter **23**, 464204 (2011) (5 pp.)
- Zapf, S., Wu, D., Bogani, L., Jeevan, H.S., Gegenwart, P., Dressel, M.: Phys. Rev. B **84**, 140503(R) (2011)
- Ryan, D.H., Cadogan, J.M., Xu, S., Xu, Z., Cao, G.: Phys. Rev. B **83**, 132403 (2011)
- Maeter, H., Luetkens, H., Pashkevich, Yu.G., Kwadrin, A., Khasanov, R., Amato, A., Gusev, A.A., Lamonova, K.V., Chervinskii, D.A., Klingeler, R., Hess, C., Behr, G., Büchner, B., Klauss, H.H.: Phys. Rev. B **80**, 094524 (2009)
- Jesche, A., Caroca-Canales, N., Rosner, H., Borrmann, H., Ormeci, A., Kasinathan, D., Klauss, H.H., Luetkens, H., Khasanov, R., Amato, A., Hoser, A., Kaneko, K., Krellner, C., Geibel, C.: Phys. Rev. B **78**, 180504(R) (2008)
- Uhoya, W., Tsoi, G., Vohra, Y.K., McGuire, M.A., Sefat, A.S., Sales, B.C., Mandrus, D., Weir, S.T.: J. Phys. Condens. Matter **22**, 292202 (2010)
- Ni, B., Abd-Elmeguid, M.M., Micklitz, H., Sanchez, J.P., Vulliet, P., Johrendt, D.: Phys. Rev. B **63**, 100102 (2001)